Comparison of Satellite-Derived and In-Situ Observations of Ice and Snow Surface Temperatures over Greenland

Dorothy K. Hall[1], Jason E. Box[2], Kimberly A. Casey[3], Simon J. Hook[4], Christopher A. Shuman[5] and Konrad Steffen[6]

[1]Cryospheric Sciences Branch, Code 614.1
NASA Goddard Space Flight Center
Greenbelt, MD 20771
dorothy.k.hall@nasa.gov

[2]Department of Geography, The Ohio State University,
1036 Derby Hall, 154 North Oval Mall, Columbus, OH 43210-1361

[3]RS Information Systems, Inc., 1651 Old Meadow Road, McLean, VA 22102

[4]Jet Propulsion Laboratory, California Institute of Technology, Pasadena, CA, 91109

[5]Goddard Earth Science and Technology Center, University of Maryland Baltimore County, 5523 Research Park Dr., Suite 320, Baltimore, MD 21228

[6]Cooperative Institute for Research in Environmental Sciences
University of Colorado, Boulder, CO 80309-0216

ABSTRACT

The most practical way to get a spatially broad and continuous measurements of the surface temperature in the data-sparse cryosphere is by satellite remote sensing. The uncertainties in satellite-derived LSTs must be understood to develop internally-consistent decade-scale land-surface temperature (LST) records needed for climate studies. In this work we assess satellite-derived "clear-sky" LST products from the Moderate Resolution Imaging Spectroradiometer (MODIS) and the Advanced Spaceborne Thermal Emission and Reflection Radiometer (ASTER), and LSTs derived from the Enhanced Thematic Mapper Plus (ETM+) over snow and ice on Greenland. When possible, we compare satellite-derived LSTs with in-situ air-temperature observations from Greenland Climate Network (GC-Net) automatic-weather stations (AWS). We find that MODIS, ASTER and ETM+ provide reliable and consistent LSTs under clear-sky conditions and relatively-flat terrain over snow and ice targets over a range of temperatures from -40 to 0°C. The satellite-derived LSTs agree within a relative RMS uncertainty of ~0.5°C. The good agreement among the LSTs derived from the various satellite instruments is especially notable since different spectral channels and different retrieval algorithms are used to calculate LST from the raw satellite data. The AWS record in-situ data at a "point" while the satellite instruments record data over an area varying in size from: 57 X 57 m (ETM+), 90 X 90 m (ASTER), or to 1 X 1 km (MODIS). Surface topography and

other factors contribute to variability of LST within a pixel, thus the AWS measurements may not be representative of the LST of the pixel. Without more information on the local spatial patterns of LST, the AWS LST cannot be considered valid ground truth for the satellite measurements, with RMS uncertainty ~2°C. Despite the relatively large AWS-derived uncertainty, we find LST data are characterized by high accuracy but have uncertain absolute precision.

INTRODUCTION AND BACKGROUND

Recently, there has been a great deal of attention on the increasing temperatures in the Arctic due to observed and projected warming (IPCC, 2007) and the positive ice-albedo feedback. Climate models predict continued Arctic warming but they differ in their predictions of the extent, rate and magnitude of the temperature increases. The most practical way to get a spatially broad and continuous measurement of surface temperature of the cryosphere is through satellite remote sensing. The uncertainties in satellite-derived land-surface temperatures (LSTs) must be understood to develop internally-consistent decade-scale LST records needed for climate studies. The level of confidence in the accuracy of LST records may be established through comparison with independent observations. LST can also be referred to as ice-surface temperature (IST) but in this work, we adopt the conventional LST terminology.

Analysis of the Advanced Very High Resolution Radiometer (AVHRR)-derived surface temperature of the Antarctic and Greenland ice sheets, ice caps and smaller glaciers provides a method to evaluate melt and climate trends over about the last three decades. These measurements can be used as a surrogate for, and in addition to, air-temperature records (Box, 2002) that are obtained from relatively few and scattered in-situ observations (Stroeve and Steffen, 1998; Wang and Key, 2003 and 2005a and b; Comiso, 2006). Satellite-derived LST data are also useful for validation of climate models and as input to data-assimilation models. North of 60°, clear-sky surface temperature has increased over about the last two decades. Based on analysis of AVHRR data acquired above the Arctic Circle, Comiso (2006) shows an increase of 0.72±0.10°C per decade from 1981 – 2005; Wang and Key (2005b) show an increase of 0.57±0.02°C per decade using the AVHRR Polar Pathfinder dataset from 1982 – 1999. Warming has not been uniform, and there are some areas of cooling during that same period, particularly over large areas of Siberia.

Thermal infrared (TIR) sensors facilitate LST and melt-condition monitoring over extensive areas (Key and Haefliger, 1992; Rees, 1993; Key et al., 1997; Stroeve and Steffen, 1998; Comiso, 2006; and Hall et al., 2004, 2006 & 2008), especially when used with complementary satellite-derived passive- and active-microwave data (e.g., see Nghiem et al., 2001). Yet a rigorous assessment of the random and systematic errors in the various satellite TIR measurements of surface temperature has not been established for snow and ice targets. LST errors derived from satellites come from a variety of sources, including: effects of very thin, unmasked clouds and atmospheric water vapor, and imprecise accounting for emissivity variations. In addition, calibration inconsistencies in the longer-term satellite record are important, especially when the same basic instrument is used on different satellites over a period of many years.

NASA's EOS provides space-borne instruments suitable for measuring snow/ice surface temperature using TIR sensors. The present study focuses on TIR

surface-temperature measurements from *standard products* derived from two satellite-borne instruments, namely: the Moderate-Resolution Imaging Spectroradiometer (MODIS) and the Advanced Thermal Emission and Reflection Radiometer (ASTER), both on the EOS Terra satellite. We also include LSTs derived from the Enhanced Thematic Mapper Plus (ETM+) on the Landsat-7 satellite. These sensors have different spatial resolutions and spectral channels; in addition, different algorithms are used to derive surface temperature. Though MODIS and ASTER LSTs have been compared in many previous studies [see for example, Jacob et al. (2004), Schmugge and Ogawa (2006) and Mihalcea et al. (2007)], the studies have not focused on the cryosphere. To our knowledge, no study has been published in the peer-reviewed literature that compares multiple snow and ice LSTs derived from the various Earth Observing System (EOS) standard products.

One way to assess the accuracy of remotely-sensed LSTs is to compare the values with in-situ LSTs. Various factors make that a difficult task including the fact that the in-situ observations are point measurements while the satellite-derived observations represent LSTs from a much larger area. Also, in-situ observations from weather stations, and in particular automatic weather stations (AWS) are generally acquired at some height above the surface so that the measured air temperature must be extrapolated to a surface temperature, or LST. That calculation is also affected by meteorological factors such as wind speed, but for higher wind-speed conditions, near-surface air temperature is very close to the surface temperature.

Standard LST products, available from the Land Processes Distributed Active Archive at the EROS Data Center in Sioux Falls, South Dakota, are available from both the MODIS and ASTER instruments. These products were developed and validated using a specific algorithm that is community-endorsed for use with a specific sensor. Though other products may also be available, the standard products are usually maintained by the investigator who developed the algorithm. A great deal of documentation and quality-control information is available for the products from the product developers and the EROS Data Center. The validation presented in the present paper is useful for assessing the errors of these commonly-used products. Though there is no standard LST product from the ETM+ instrument, we use the formulation of Barsi et al. (2005) to calculate the LST.

In this paper, we assess LSTs from MODIS and ASTER standard products (MOD11_L2 and MOD11A1, and AST08), and LSTs from ETM+ for snow and ice targets on the Greenland Ice Sheet, and ice caps located outside the margins of the ice sheet. We use in-situ air-temperature data from Greenland Climate Network (GC-Net) AWS (Steffen et al., 1996; Steffen and Box, 2001) (Figure 1) to compare with satellite-derived LSTs. It is not the intent of this work to derive more accurate LSTs nor to modify or “improve” existing algorithms, rather, we are comparing satellite-derived LSTs relative to each other and, relative to in-situ

measurements, to improve our understanding of the uncertainties in, and the limitations of, these data products. These commonly-used products are increasingly considered for uses in climate-data records (CDRs), thus the uncertainties must be established.

THEORETICAL BASIS FOR REMOTE SENSING IN THE MID- AND THERMAL-INFRARED TO RECOVER SNOW AND ICE SURFACE TEMPERATURES

Mid-IR and TIR-remote sensing is based on measurement of the radiance emitted from the surface and modified by the atmosphere, with a goal to recover the kinetic temperature and emissivity from the measured at-sensor radiance. The at-sensor radiance (*Ls*) for a given wavelength (λ) in the mid or TIR, excluding any reflected solar contribution in the mid IR, can be written as:

$$Ls_\lambda = [\, \varepsilon_\lambda L_{bb\lambda}(T) + (1 - \varepsilon_\lambda) L_{sky\lambda} \,] \tau_\lambda + L_{atm\lambda} \qquad [1]$$

where:

ε_λ = surface emissivity at wavelength λ.

$L_{bb\lambda}(T)$ = spectral radiance from a blackbody at surface temperature *T*.

$L_{sky\lambda}$ = sky radiance (spectral downwelling radiance incident upon the surface from the atmosphere.)

τ_λ = transmittance (spectral atmospheric transmission.)

$L_{atm\,\lambda}$ = path radiance (spectral upwelling radiance from atmospheric emission and scattering that reaches the sensor.)

The effect of τ_λ is to reduce the amount of ground-emitted radiance measured at the sensor; $L_{atm\,\lambda}$ adds a component unrelated to the ground and $L_{sky\lambda}$ serves to reduce the spectral contrast. Any surface radiance, temperature, or emissivity retrieval must compensate for atmospheric effects.

The surface temperature (*T*) is not an intrinsic property of the surface; it varies with external factors such as meteorological conditions. Emissivity *is* an intrinsic property of the surface and is independent of the temperature. See Hook et al. (2007) for further discussion.

Surface emissivity

The surface emissivity is defined as the ratio of the actual radiance emitted by a given surface to that emitted by a black body at the same kinetic temperature. Salisbury et al. (1994) show that snow emissivity departs significantly from black body behavior in the 8 – 14 μm part of the spectrum. Emissivity of snow varies with liquid water content and snow grain size especially at larger grain sizes

(Salisbury et al., 1994; Wald, 1994; Hori et al., 2006). Grain sizes on the surface of the Greenland Ice Sheet do not vary much due to redistribution of surface snow by the wind, allowing a constant grain size (0.3 – 0.5 mm) to be an appropriate assumption for non-melting snow according to Stroeve et al. (1996). [Other, special circumstances, can cause the surface snow-grain size to increase when, for example, surface hoar forms with centimeter-size snow grains (Shuman and Alley, 1993)].

Emissivity is also sensitive to sensor viewing angle (Dozier and Warren, 1982; Salisbury et al., 1994; Hori et al., 2006). Fine- and medium-grained snow exhibits only a slight angular dependence, but the angular dependence increases for coarse-grained snow, especially at the larger viewing angles (e.g., 75°). Bare ice exhibits the largest angular dependence, showing a decrease in emissivity with increasing viewing angle (Hori et al., 2006). Also see Dozier and Warren (1982) for modeled values of hemispherically-averaged emissivity curves of snow for grain radii from 50 – 1000 μm, and for viewing angles of 0 to 75°, and Hori et al. (2006) who reviewed and discussed those results, and Dash et al. (2002) for further discussion of land-surface temperature and emissivity estimation.

Emissivity of snow and ice features is far less variable than the range encountered in a wide variety of land surfaces, leading to greater potential accuracies in retrieved LST over snow and ice even when the emissivity is not known precisely. To obtain snow-surface temperatures to an accuracy of 0.1 K, the emissivity must be known to within 0.1% (Stroeve et al., 1996).

Spectral libraries are available that provide emissivities based on laboratory measurements (Shafer, 1971; Salisbury et al., 1994; the ASTER spectral library http://speclib.jpl.nasa.gov/); and the University of California at Santa Barbara emissivity library (http://www.icess.ucsb.edu/modis/EMIS/html/em.html)). Shafer (1971) measured the emissivity of 185 snow samples at temperatures from -1 to -18°C in the 8-14 μm wavelength range, obtaining values ranging from 0.966 to 0.989, with fresh snow having the lowest value (0.975), and crusted snow having the highest mean-measured emissivity (0.985), under clear skies. The average emissivity of all of his samples was 0.978, though more-recent works tend to report higher emissivity values (see, for example, Wan et al., 2002; Hori et al., 2006).

SATELLITE INSTRUMENTS

MODIS

The Terra satellite was launched in December 1999, and the Aqua satellite was launched in May 2002, both having MODIS instruments in their payload. The Terra and Aqua MODIS instruments are effectively the same, although band 31 (11 μm) on the Aqua MODIS saturates at temperatures about 60K below those

for Terra (~400K). (In addition, the Aqua MODIS near-infrared band 6 is non-functional.)

The MODIS instrument acquires data in 36 spectral channels (Barnes et al.,1998; Salomonson et al.,1989). MODIS scans ± 55° from nadir and provides daytime and nighttime imaging of any point on the Earth every 1-2 days. Channels 31 and 32 centered on 11.03 and 12.02 μm, respectively, are used to produce the LST products that are used in this study (Table 1). MODIS IR radiances are quantized in 12 bits and have a ground resolution of 1 km at nadir. MODIS IR radiances are calibrated with a cold space view and full aperture black body viewed before and after each Earth view.

ASTER

The ASTER instrument on the Terra satellite acquires radiances in 14 spectral channels as part of three sensor sub-systems. Channels 10-14 of the TIR subsystem (between 8.15 and 11.65 μm) are used to produce the product that is used in this study (Table 1). The TIR data are quantized in 12 bits, have a spatial resolution of 90 m at nadir and are calibrated with a full-aperture temperature-controlled black body. The black body is viewed before and after each data acquisition and periodically heated to obtain calibration data at different temperatures. The TIR subsystem utilizes a whiskbroom scanner that can be pointed ± 8.55° across track allowing any coordinate on Earth to be imaged as frequently as every 16 days.

ETM+

The Landsat-7 ETM+ is also part of the EOS suite of satellites. Landsat-7 was launched in April 1999, and has eight bands ranging from 0.45 to 12.5 μm; the ground resolution ranges from 15 m in the panchromatic band to 57 m in the single TIR band (Table 1), from which LST may be calculated. The ETM+ scan-line corrector failed in June 2003 rendering subsequent ETM+ data useless for the present work.

Ice and Cloud Elevation Satellite (ICESat)

The ICESat satellite, launched in January 2003, carries a single instrument, the Geoscience Laser Altimeter System (GLAS), which was designed to use laser pulses at 1064 and 532 nm to map the surface topography of Earth precisely and to sound the atmosphere. The primary ICESat mission is to provide detailed surface-elevation data of the ice sheets, to improve ice-sheet mass-balance assessments and enable volumetric change monitoring (Zwally et al., 2002). For this work, we use ICESat-derived elevations along transects across two ice caps (Flade Isblink and North Ice Cap) outside the margins of the Greenland Ice Sheet to study variation in LST as a function of elevation.

INSTRUMENT SPECIFIC LAND-SURFACE TEMPERATURE (LST) ALGORITHMS, PRODUCTS AND GROUND MEASUREMENTS

The methodology used to derive LST varies from MODIS, ASTER and ETM+, as the different methods take advantage of the unique characteristics of each sensor. The accuracy of both the split-window and single-channel methods, discussed below, relies on knowledge of the surface emissivity and atmospheric temperature and humidity. Because snow/ice emissivity does not vary widely, these conventional methods produce useful snow/ice LSTs at the upper limit of accuracy.

MODIS products

We use the LST Collection 4 (or Version 4 (V4)) product suite (MOD11 and MYD11) developed by Wan et al. (2002); also see Wan (2008). (MOD refers to a Terra MODIS product and MYD refers to an Aqua MODIS product.) We use only Terra MODIS products because there are more opportunities for comparison with other data since the Terra MODIS has been operating longer than the Aqua MODIS. Furthermore, Terra has an overpass time (14:30-16:30 UTC) for Greenland within 2 hours of local solar noon. Also, MODIS and ASTER are both flown on the Terra spacecraft, so it is often easy to find MODIS scenes when ASTER scenes are available.

The Terra MODIS 1-km resolution LST algorithm produces a swath product (MOD11_L2) that is based on the generalized split-window technique (Wan and Dozier, 1996) using MODIS bands 31 and 32 (Table 1). To determine the actual LST from an instrument that has two IR channels, one must correct for absorption and reemission of radiation by atmospheric gases, predominately water vapor. The “split-window” method is widely used to achieve some correction for atmospheric effects because the measured temperature difference between the two IR channels, in a “split-window” algorithm, is proportional to the amount of water vapor in the atmosphere. To compute the LST using MOD11_L2, the emissivity must be prescribed. For bands 31 and 32, the emissivities used in the algorithm to compute LST over the Greenland Ice Sheet, are 0.993 (for band 31) and 0.990 (for band 32), and do not vary seasonally. The daily 1-km LST product (MOD11A1) is developed from the swath product. MOD11A1 is provided on a sinusoidal grid.

Wan and Dozier (1996) calculated coefficients in the generalized split-window LST algorithm by interpolation on a set of multidimensional look-up tables obtained by linear regression of MODIS simulation data from radiative-transfer calculations over a wide range of surface and atmospheric conditions. The coefficients depend on column water vapor and surface air-temperature values from the MODIS atmosphere-profile standard product, MOD07 (Seemann et al.,

2006). The MODIS Atmospheric Profile product consists of several parameters: total-ozone burden, atmospheric stability, temperature and moisture profiles, and atmospheric water vapor. All of these parameters are produced day and night for Level 2 at a resolution of 5x5 1-km pixels when at least nine FOVs are cloud free. The following MODIS products are input to the MOD11_L2 algorithm: sensor radiance (MOD021km), geolocation (MOD03), cloud mask (MOD35_L2), atmospheric temperature and water vapor (MOD07_L2), land-cover (MOD12Q1) and snow-cover (MOD10_L2).

The swath-based LST product (MOD11_L2) was used in the present work when it was necessary to know the exact time that the data were acquired to synchronize image data and to coordinate with ground and other satellite observations. The daily LST product (MOD11A1) was used in the transects across the two ice caps where knowledge of exact time-of-day was not needed because the ice cap surfaces were at the melting point.

ASTER products

ASTER produces one emissivity product (AST05) and a separate surface temperature product (AST08). The emissivity product contains five bands corresponding to the surface emissivity at the wavelengths of the five TIR bands. The data are in swath (scene) format. A more detailed description of the ASTER instrument, products and their application is given in Yamaguchi et al. (1998). For this work, we used the AST08 products downloaded between 25 July 2006 and 3 October 2007.

The ASTER algorithm to derive LST and emissivity uses a radiative transfer model to correct the at-sensor radiance to surface radiance followed by an emissivity model to separate the surface radiance into temperature and emissivity. The ASTER LST algorithm requires atmospheric profiles from either satellite sounding or conventional weather balloon soundings made twice-daily, globally, for the atmospheric model (Price, 1983; Susskind et al. 1984; Chedin et al. 1985) and an emissivity model that is typically based on laboratory and field measurements (Kealy and Hook, 1993; Matsunaga, 1994). In this approach, a temperature-independent index is calculated showing the range, that is minimum-maximum difference (MMD) in emissivity with wavelength, but not the absolute value. A calibration curve is then derived using laboratory data that allows the observed variation (or MMD) to be used to obtain the unknown absolute emissivity value.

Once the unknown emissivity value is obtained, Equation 1 can be used to obtain the temperature and emissivities for the other bands. Rocks and soils have a large MMD whereas vegetation and snow have a small MMD. This is because within the TIR range, rocks and soils show strong emissivity variation, whereas the emissivity of snow and ice is more consistent, varying between about 0.97

and 1.0. The calibration-curve approach is used to recover LST and emissivity from ASTER (Gillespie et al., 1998 and1999).

ETM+ derived LST

A separate atmospheric correction must be done, and the target emissivity must be prescribed, as in Barsi et al. (2003 and 2005), to derive LST from the single TIR band on the ETM+. Ancillary data are needed to adjust the top-of-atmosphere (TOA) brightness temperature to a surface skin temperature, or LST. An atmospheric-correction tool was developed by Barsi et al. (2005) for the Landsat-5 Thematic Mapper (TM) and Landsat-7 ETM+ thermal channels, and is accessible through http://atmcorr.gsfc.nasa.gov. Date, time and location of the Landsat scene are input by the user. The atmospheric-correction parameter calculator uses National Centers for Environmental Prediction (NCEP) modeled global atmospheric profiles as input data, along with MODTRAN and other integration algorithms, to derive site-specific atmospheric transmission and upward and downward radiances for the given Landsat scene. Using the atmospheric-correction parameter output, a series of calculations is performed to derive a surface kinetic temperature for each pixel in the Landsat scene. The first calculation involves converting the digital number, DN, to the TOA spectral radiance, R (see Markham and Barker, 1985). Then the formulation of Barsi et al. (2005) is used to perform the atmospheric correction, deriving the surface-leaving radiance, R. Finally, conversion of radiance to LST can be made using a sensor-specific approximation to Planck's function.

$$T = K2 / \log [(K1/R) + 1] \qquad [2]$$

Where T is surface temperature in Kelvins, and K2 and K1 are calibration constants in Kelvins, and in W m^{-2} sr^{-1} μm^{-1}, respectively (Markham and Barker, 1985).

Greenland Climate Network (GC-Net) Automatic Weather Stations (AWS)

The GC-Net AWS network (Figure 1) has collected weather and climate information on the Greenland Ice Sheet since 1995 (Steffen et al., 1996; Steffen and Box, 2001) [http://cires.colorado.edu/science/groups/steffen/gcnet/]. Each AWS is equipped with instruments to sample micro-meteorological variables used to obtain surface energy and mass budget closure. Air temperature is measured at two heights within 5 m of the surface with 1.2 m separation using thermocouples and thermistors in passively-ventilated solar radiation shields. Samples are obtained at 15 or 60 second intervals. Hourly average data are transmitted via a satellite link throughout the year. Other measured parameters include: wind speed and direction, air humidity, air pressure, surface

accumulation rate, and surface radiation balance in broadband shortwave and TIR wavelengths.

Continuous near-surface air temperature and LST records have been acquired for more than two years at the Summit AWS site using a Vaisala CS-500 Type-E TIR thermocouple sensor to record air temperature and a Vaisala Type-T thermocouple TIR sensor that was placed 10 cm above the surface to record the surface temperature as one of the GC-Net AWS stations (http://cires.colorado.edu/science/groups/steffen/gcnet/) assuming a snow emissivity of 0.99. An absolute accuracy for LST was found to be ±0.2°C (r^2 = 0.98) at the Summit site (Figure 2) where a mean warm bias of 1.0°C was evident in 16,123 hourly samples. The surface temperatures were derived from two positions on an AWS mast with actively-ventilated air temperature sensors. Field and laboratory calibrations of the thermocouple devices are generally conducted annually and the resulting corrections are typically <3% (Steffen et al., 1996; Steffen and Box, 2001).

METHODOLOGY AND RESULTS

To assess the accuracy of MODIS and ASTER LST standard-data products, and LSTs derived from the ETM+, first we compared satellite-derived LSTs along transects across ice caps on Greenland that were experiencing surface melt across the entire ice cap. We then compared MODIS, ASTER and ETM+ LSTs of the ice sheet with AWS-derived LSTs when possible at a variety of surface temperatures. Finally, we compared MODIS and ASTER, and MODIS and ETM+ LSTs in the absence of in-situ observations, at surface temperatures ranging from about -16 to 0°C.

Transects

Transects over two ice caps in Greenland (located outside the margins of the ice sheet), Flade Isblink and North Ice Cap, were studied using MODIS and ASTER LST products, and ICESat altimetry data (Figures 3a and 3b). On the image dates (3 July 2001 and 23 June 2004), LSTs do not vary with elevation (derived from ICESat), thus the entire ice surface is approximately at the melting point (Figure 3a). The mean LST of Flade Isblink (not shown) on 3 July 2001 is 0.84±0.70°C (n = 1,564,335), as determined from ETM+ (where the value 0.98 was input as the emissivity), and 0.47±0.26°C (n = 21,843), as determined from MODIS (MOD11A1), an insignificant difference of only 0.37±0.44°C. MODIS and ASTER LSTs agree over North Ice Cap (23 June 2004) within ~±0.8°C (Figure 3b). Agreement is also about ~±0.8°C between the satellite-derived LSTs and the surface if we assume that the surface is at 0°C.

Comparisons of satellite-derived LSTs with GC-Net AWS-derived measurements

First, scenes were selected manually from the various instruments that were acquired on the same day, and at the same time (when possible). We searched for relatively-flat areas as close to nadir as possible, to minimize angular effects. Pixels from each scene were selected from homogeneous parts of the scene as determined from visual (textural) analysis, and in areas with no obvious clouds or fog. The LST value from one MODIS pixel was compared to mean LSTs of the same area from the ASTER and ETM+ scenes.

We used the LST value from the MODIS pixel (MOD11_L2) corresponding to the location of the AWS and the time of the AWS measurement. Initially, we examined LST image pairs over the Greenland Ice Sheet and in-situ data from nine stations in the AWS network (Figure 4) for a total of 11 cases. The number of ETM+ pixels used to calculate the mean LST increases with distance from nadir, corresponding with the increasing size of the MODIS pixel away from nadir. Ten of the cases involved comparing MODIS and ETM+ LSTs with an AWS-derived LST, and one case (2 July 2001) involved comparing ASTER and ETM+ LSTs with the corresponding AWS-derived LST. (The MODIS LST product was not available on 2 July 2001.) In that one case where near-simultaneous ASTER and ETM+ were compared with the AWS-derived LST from Summit station, we used just one ASTER and one ETM+ pixel, the pixels that corresponded most closely with the location of the AWS. Since it was not always possible to get the times of the satellite-scene acquisitions and AWS acquisition of LST within an hour of each other, the AWS-derived air temperatures were interpolated between acquisition times to provide a more-accurate comparison with the time of acquisition of the MODIS LSTs (see Table 2).

For the cases shown in Table 2, the LSTs derived from different satellite instruments are in better agreement than they are with the AWS LSTs. Also, the satellite-derived LSTs agree in sign in most cases (Figure 4).

MOD11_L2 LST comparison with AWS observations. A collection of 121,506 hourly-average cases from 15 GC-Net AWS (Figure 1) over the 1998-2001 period are used to evaluate the near-surface (below ~5 m) temperature gradient $(\Delta T/\Delta z)$ to model LST. $\Delta T/\Delta z$ is measured using $T_2 - T_1$, where T_2 is farther from the surface than T_1. Δz is the instrument spacing: $z_2 - z_1$, is equal to 1.2 m in most cases. The magnitude of $\Delta T/\Delta z$, that is, the near-surface *thermal stratification* varies with surface radiation balance and micro-meteorological conditions. Under clear-sky conditions, the strongest modulators of $\Delta T/\Delta z$ are downward solar irradiance (S↓) and wind speed. When S↓ is small, surface emitted IR radiation exceeds absorbed solar irradiance and the surface cools more than the air above the surface leading to a *temperature inversion*, that is, $\Delta T/\Delta z > 0$. Wind speed facilitates turbulent mixing of heat downward under inversion cases where it is lost by upward IR emission. During air *temperature lapse* conditions, the surface has been heated, usually by S↓ such that turbulent mixing moves heat away from the surface leading to negative $\Delta T/\Delta z$. Strong

winds can neutralize $\Delta T/\Delta z$ even when surface solar heating is large. A clear signal (r=-0.987) of decreasing temperature inversion strength with increasing downward solar irradiance is evident. Below 20 W m^{-2}, on average, $\Delta T/\Delta z$= +0.33 K m^{-1}. On average, inversion becomes lapse for downward solar irradiance exceeding 350 W m^{-2}. The gradient in $\Delta T/\Delta z$ with S↓ is -0.90 K m^{-1} kW^{-1}. Thus, the lapse rate at 800 W m^{-2} = -0.40 K m^{-1}.

Figure 5 illustrates the comparison between MODIS-derived LST and AWS air temperature with and without cases associated with large AWS air temperature uncertainty, that is, when downward solar irradiance exceeded 240 W m^{-2}, wind speed was < 4 m s^{-1}, and air temperatures above the melting point. When neutral thermal stratification (that is, $|\Delta T/\Delta z|$ < 0.1 K m^{-1}) conditions prevail, nominal height air temperature may be used as an LST surrogate because air temperatures and LSTs are equivalent within the specified accuracy (~0.1 K) of the AWS air temperature sensors.

Estimating LST by extrapolation during strong $\Delta T/\Delta z$ cases is not useful for the MOD11_L2 accuracy assessment. It is only under small absolute $\Delta T/\Delta z$ that an insignificant MODIS LST error is evident.

It was not possible to compare significant numbers of ASTER and ETM+ -derived LSTs with corresponding AWS-derived LSTs (as was done with MODIS) due to our inability to locate an adequate number of cloud-free ASTER and ETM+ scenes coincident with automatic weather stations.

Comparison of Satellite-Derived LSTs

ASTER and ETM+ LSTs were compared with MODIS LSTs in the absence of in-situ measurements. These results provide additional information on how well the independently-derived LSTs agree over a range of ice-surface temperatures (also see Figures 3a and b for additional cases when LSTs were near 0°C), even though different instruments, algorithms and channels are used to derive the LSTs. Points were selected from a range of elevations on the ice sheet and in different seasons, covering a range of surface temperatures from about -16 to 0°C.

ASTER- and MODIS-derived LSTs agree, with r^2 = 0.97 and RMSE = 0.54°C (n = 65). The mean bias = 0.22°C, with the ASTER LSTs being slightly higher than the MODIS LSTs (Figure 6).

Results of the MODIS and ETM+ comparisons are shown in Figures 7a and b. Two different emissivity values were input to the ETM+ algorithm and were selected based on the literature survey. Using an emissivity value of 0.98 as an input to the ETM+ algorithm, r^2 = 1.0, (RMSE = 0.34°C, mean bias = 0.07°C (n = 80), with ETM+ values being slightly higher than MODIS values. When an

emissivity = 0.99 was input to the ETM+ algorithm, r^2 = 0.99, RMSE = 0.56°C and mean bias = -0.43°C (n = 80), with ETM+ values being slightly lower than MODIS values. Though the correlation between ETM+ and MODIS LSTs is approximately the same and very high (r=1.0), the mean bias and RMSE are both lower when using an emissivity value of 0.98 (as compared to when emissivity = 0.99 was used). Implicit in that, however, is the assumption that the MODIS LSTs are the "truth," but we have no way of knowing that, given the data that we have available.

ADDITIONAL CONSIDERATIONS

Clouds

The satellite-derived LSTs represent "clear-sky" surface temperatures. 'Clear sky' is determined from the MODIS cloud mask (Ackerman et al., 2002) for the MODIS products used in this work. Though we studied each scene visually to confirm that the selected points were not cloud contaminated, undetected thin clouds and a varying atmospheric water vapor column may also influence the accuracy of satellite LST retrievals. Incorporating information from other sensors, such as the Atmospheric Infrared Sounder (AIRS) instrument could help constrain error from unidentified thin cloud and atmospheric water vapor radiative effects. A cloud-clearing algorithm that uses texture and time-variance might also be useful such as that reported by Shi et al. (2007) using the MODIS and Multi-angle Imaging Radiometer (MISR), both flown on the Terra satellite.

Over Greenland, the effect of water vapor absorption on the brightness temperature in MODIS band 31 (Table 1) is estimated to be within ±1K in the winter, and greater (2-3K) in the summer and in southern Greenland, especially around the coast. When the atmospheric temperature is higher than the LST, the atmospheric effect may increase the brightness temperature (Z. Wan, written communication, 2008).

Angular effects

Angular effects that may influence the accuracy of the MODIS LST retrievals were not studied in this work, nor were effects associated with rugged terrain. Based on modeling by Dozier and Warren (1982), Key and Haefliger (1992) show the emissivity variations by scan angle for the AVHRR channel 4 (11μm). For example, the emissivity varies from 0.9988 at a scan angle of 0°, to 0.9955 at a scan angle of 50°. However, the effect of scan angle is greater with coarse-grained snow and bare ice (Hori et al., 2006). In addition, ice-sheet topography can influence the emissivity and thus the accuracy of the LST retrieval. Though we attempted to select only relatively-flat areas, areas on the ice sheet that

appear flat from above can actually have significant local topography, that is, with a topographic undulation amplitude of >20 m.

How representative are the AWS measurements?

The AWS "point" measurements may fail to represent the surface temperature over the area of the 1 km x 1km (MODIS), 90 m x 90 m (ASTER) or 57 m x 57 m (ETM+) pixels, especially in instances where wind speed is low and surface slope heterogeneity is relatively large. One author (K. Steffen) has made LST measurements over a 1-km area at Swiss Camp on the Greenland Ice Sheet and found surface-temperature variability on the order of ~1°C. The temperature variability was attributed to surface roughness (typically 10-15 cm in amplitude and several meters in wavelength) and some shadowing. Additional surface LST observations need be made in a local array to evaluate spatial variability in LST, over areas corresponding with satellite pixels. Without more information on the local spatial patterns of LST, the AWS LST cannot be considered absolute ground truth for the satellite measurements.

SUMMARY AND CONCLUSIONS

MODIS and ASTER products, and ETM+ derived LST provide reliable and consistent LSTs under clear-sky conditions and relatively-flat terrain over snow and ice targets over a broad temperature range of -40 to 0°C. The satellite-derived LSTs agree better with each other than they do with the GC-Net AWS-derived LSTs even though different algorithms are used with each instrument to calculate LST.

The agreement between MODIS (MOD11_L2) and ASTER (AST08) LSTs is very good over the Greenland Ice Sheet, with r^2 = 0.97 and RMSE = 0.54°C (n = 65). The agreement is even better between MODIS and ETM+ especially when an emissivity = 0.98 was input to the algorithm to calculate LST, with r^2 = 1.0 and RMSE = 0.34°C (n = 80).

We have demonstrated the difficulty in validating LST measurements from satellites using in-situ measurements even over a relatively homogeneous land surface such as an ice sheet. Careful selection of AWS data was necessary to obtain a reliable set of in-situ data to compare with the satellite data. The average bias of satellite-derived and in-situ LSTs (-0.3 °C) is well within the RMS error of 2.1°C (n = 48). Without more information on the local spatial patterns of LST, the AWS air-temperature-derived LSTs cannot be considered absolute ground truth for the satellite measurements because the AWS record data at one "point," while the satellite instruments record data in a pixel varying in size from 57 X 57 m (ETM+), 90 X 90 m (ASTER) or 1 X 1 km (MODIS). Surface

topography and other factors contribute to variability of LST within a pixel, thus the AWS measurements are often not representative of the entire pixel.

It is not possible from this work to determine which LST product or measurement provides the highest accuracy, or which LST algorithm is the most robust. An extensive network of surface-temperature measurements, coincident with satellite overpasses, is required to answer those questions.

In the future, the National Polar-orbiting Operational Environmental Satellite System (NPOESS) Visible/Infrared Imager/Radiometer Suite (VIIRS) will be launched with IR channels and an LST product will be produced. Other instruments may also be launched that will provide LST measurements or products. To facilitate the production of data records that will be developed using multiple instruments and perhaps even climate-data records (CDRs) over snow and ice targets, uncertainties in LST retrieval must be established. The use of internally-consistent products will permit determination of “clear-sky” surface-temperature trends (if any) to be detected and monitored in the polar regions for climate and other studies. As such, when the data are applied in climatological analyses, trends should exceed our calculated RMS errors to be considered ‘significant’ within the observational capability.

ACKNOWLEDGMENTS

The authors thank Joe Nigro / SSAI, for earlier work with ETM+ LST calculations, and Nick DiGirolamo and George Riggs / SSAI, who provided invaluable programming support. We also thank Julia Barsi / SSAI, for discussions regarding the ETM+ LST algorithm, and Tom Schmugge of New Mexico State University, for discussions regarding the ASTER LST product. The research described in this paper was carried out in part at the Jet Propulsion Laboratory, California Institute of Technology, under a contract with NASA. This research was supported by NASA’s Cryospheric Sciences Program.

REFERENCES

Ackerman, S.A., Strabala, K.I., Menzel P.W.P., Frey, R.A., Moeller, C.C. & Gumley, L.E. (1998). Discriminating clear sky from clouds with MODIS. *Journal of Geophysical Research* 103(D24):32,141-32,157.

Barsi, J.A., Barker, J.L. & Shott, J.R. (2003). An atmospheric correction parameter calculator for a single thermal band Earth-sensing instrument, *Proceedings of IGARSS 2003*, Centre de Congress Pierre Bandis, Toulouse, France, 21-25 July 2003.

Barnes, W.L., Pagano, T.S. & Salomonson, V.V. (1998). Prelaunch characteristics of the Moderate Resolution Imaging Spectroradiometer (MODIS) on EOS-AM1, *IEEE Transactions on Geoscience and Remote Sensing,* 36(4):1088-1100.

Barsi, J.A., Shott, J.R., Palluconi, F.D. & Hook, S.J. (2005). Validation of a Web-based atmospheric correction tool for single thermal band instruments, *Proceedings of SPIE*, 5822 (SPIE, Bellingham, WA, 2005), doi: 10.1117/12.619990.

Box, J. E. (2002). Survey of Greenland instrumental temperature records: 1873-2001, *International Journal of Climatology, 22*:1829-1847.

Chedin, A., Scott, M. A., Wahiche, C. & Moulinier, P. (1985). The improved initialization inversion method: a high resolution physical method for temperature retrievals from the TIROS-N series. *Journal of Climate and Applied Meteorology*, 24:124-143.

Comiso, J.C. (2006). Arctic warming signals from satellite observations, *Weather, 61(3)*:70-76.

Dash, P., Göttsche, F.-M., Olesen, F.-S. & Fischer, H. (2002). Land surface temperature and emissivity estimation from passive sensor data: theory and practice – current trends, *International Journal of Remote Sensing,* 23(13):2563-2594.

Dozier, J. & Warren, S. (1982). Effect of viewing angle on the infrared brightness temperature of snow, *Water Resources Research,* 18(5):1424-1434.

Duyrgerov, M.B. & Meier, M.F. (2000). Twentieth century climate change: evidence from small glaciers, *PNAS,* 97(4):1406-1411.

Gillespie, A.R., Rokugawa, S., Matsunaga, T., Cothern, J.S., Hook, S. & Kahle, A.B. (1998). A temperature and emissivity separation algorithm for Advanced

Spaceborne Thermal Emission and Reflection Radiometer (ASTER) images, *IEEE Transactions on Geoscience and Remote Sensing,* 36:1113-1126.

Gillespie, A., Rokugawa, S. Hook, S.J., Matsunaga, T. & Kahle, A.B. (1999). The ASTER Temperature/Emissivity Separation Algorithm Theoretical Basis Document (ATBD-AST-03) Version 2.4.

Hall, D.K., Williams, R.S., Jr., Steffen, K. & Chien, J.Y.L. (2004) Analysis of summer 2002 melt extent on the Greenland Ice Sheet using MODIS and SSM/I data. *Proceedings of the IEEE Geoscience and Remote Sensing Symposium,* 20-24 September 2004, Anchorage, Alaska.

Hall, D.K., Williams, R.S., Jr., Casey, K.A., DiGirolamo, N.E. & Wan, Z. (2006). Satellite-Derived, Melt-Season Surface Temperature of the Greenland Ice Sheet (2000-2005) and its Relationship to Mass Balance, *Geophysical Research Letters*, 33, L11501, doi:10.1029/2006GL026444.

Hall, D.K., Williams, R.S., Jr., Luthcke, S.B. & DiGirolamo, N.E. (2008). Greenland Ice Sheet surface temperature, melt and mass loss: 2000 – 2006, *Journal of Glaciology*, 54(184): 81-93.

Hook, S. J., Vaughan, R.G., Tonooka, H. & Schladow, S.G. (2007). Absolute Radiometric In-Flight Validation of Mid Infrared and Thermal Infrared Data From ASTER and MODIS on the Terra Spacecraft Using the Lake Tahoe, CA/NV, USA, Automated Validation Site. *IEEE Transactions Geoscience and Remote Sensing*, vol. 45, pp. 1798-1807.

Hori, M., Aoki, T., Tanikawa, T., Motoyoshi, H., Hachikubo, A., Sugiura, K., Yasunari, T.J., Eide, H., Storvold, R., Nakajima, Y. & Takahashi, F. (2006). In-situ measured spectral directional emissivity of snow and ice in the 8 – 14 μm atmospheric window. *Remote Sensing of Environment,* 100:486-502.

IPCC (2007). Climate Change 2007: The Physical Science Basis. Contribution of Working Group I to the Fourth Assessment Report of the Intergovernmental Panel on Climate Change, Solomon, S., D. Qin, M. Manning, Z. Chen, M. Marquis, K.B. Averyt, M.Tignor and H.L. Miller (eds.), Cambridge University Press, Cambridge, United Kingdom and New York, NY, USA.

Jacob, F., Petitcolin, F. Schmugge, T. Vermote, E. French, A. & Ogawa, K. (2004). Comparison of land surface emissivity and radiometric temperature derived from MODIS and ASTER sensors, *Remote Sensing of Environment,* 90:137-152.

Kealy. P. S. & Hook, S.J. (1993). Separating Temperature and Emissivity in Thermal Infrared Multispectral Scanner Data: Implications for Recovering Land

Surface Temperatures. *IEEE Transactions on Geoscience and Remote Sens*ing 31(6):1155-1164.

Key, J. & Haefliger, M. (1992). Arctic ice surface temperature retrieval from AVHRR thermal channels, *Journal of Geophysical Research,* 97*(D5):*5885-5893.

Key, J.R., Collins, J.B., Fowler, C. & Stone, R.S. (1997). High-latitude surface temperature estimates from thermal satellite data. *Remote Sensing of Environment, 63*:302-309.

Markham, B.L. & Barker, J.L. (1985). Spectral characterization of the Landsat thematic mapper sensors, *International Journal of Remote Sensing*, 6(5):697-716.

Matsunaga, T. (1994). A Temperature-Emissivity Separation Method Using an Empirical Relationship between the Mean, the Maximum and the Minimum of the Thermal Infrared Emissivity Spectrum. *Journal of the Remote Sensing Society of Japan*, 14(3):28-39.

Mihalcea, C., Brock, B.W., Diolaiuti, G. C., D'Agata, C., Citterio, M., Kirkbride, M.P., Smiraglia, C. & Cutler, M.E.J. (2007). Comparison of ground based and ASTER derived measurements of surface temperature and supraglacial debris thickness on Miage Glacier, Mont Blanc Massif, Italy, *Geophysical Research Abstracts*, 9, 03765.

Nghiem, S.V., Steffen, K., Kwok, R. & Tsai, W.-Y. (2001). Detection of snowmelt regions on the Greenland ice sheet using diurnal backscatter change, *Journal of Glaciology,* 47(159)*,* 539-547.

Price, J. (1983). Estimating surface temperature from satellite thermal infrared data – a simple formulation for the atmospheric effect. *Remote Sensing of Environment,* 13:353-361.

Rees, W.G. (1993) Infrared emissivities of Arctic land cover types. *International Journal of Remote Sensing,* 14(5):1013-1017.

Salisbury, J.W., D'Aria, D.M. & Wald, A. (1994). Measurements of thermal infrared spectral reflectance of frost, snow, and ice. *Journal of Geophysical Research, 99*:24,235-24,240.

Schmugge, T. & Ogawa, K. (2006). Validation of emissivity estimates from ASTER and MODIS data. *Proceedings of the 2006 IEEE International Geoscience and Remote Sensing Symposium & 27th Canadian Symposium on Remote Sensing,* Denver, Colo., 31 July – 4 August, 2006.

Seemann, S.W., Borbas, E.E., Li, J., Menzel, W.P. & Gumley, L.E. (2006). MODIS atmospheric profile retrieval algorithm theoretical basis document, online document [http://modis-atmos.gsfc.nasa.gov/_docs/MOD07:MYD07_ATBD_C005.pdf]

Shafer, B.A. (1971). Infrared temperature sensing of snow covered terrain, M.S. thesis, Montana State University, Bozeman, Mont., June, 1971, 93 p.

Shi, T., Clothiaux, E.E., Bin, Y., Braverman, A.J., Groff, D.N. (2007). Detection of daytime arctic clouds using MISR and MODIS data. *Remote Sensing of Environment,* 107:172–184.

Shuman, C. & Alley, R. (1993). Spatial and temporal characterization of hoar formation in central Greenland using SSM/I brightness temperatures, *Geophysical Research Letters, 20:*2643 – 2646.

Steffen, K., Box, J.E. & Abdalati, W. (1996). Greenland Climate Network: GC-Net, *in* Colbeck, S. C. Ed. CRREL 96-27 Special Report on Glaciers, Ice Sheets and Volcanoes, tribute to M. Meier, pp. 98-103.

Steffen, K. & Box, J. (2001). Surface climatology of the Greenland ice sheet: Greenland climate network 1995-1999, *Journal of Geophysical Research,* 106(D24):33,951-33,964.

Stroeve, J., Haefliger, M., & Steffen, K. (1996). Surface temperature from ERS-1 ATSR infrared thermal satellite data in polar regions. *Journal of Applied Meteorology, 35(8),* 1231-1239.

Stroeve, J., & Steffen, K. (1998). Variability of AVHRR-derived clear-sky surface temperature over the Greenland ice sheet, *Journal of Applied Meteorol*ogy, 37:23-31.

Susskind, J., Rosenfield, J., Reuter, D., and Chahine, M.T. (1984). Remote Sensing of weather and climate parameters from HIRS2/MSU on TIROS-N. *Journal of Geophysical Research*, 89(D3):4677-4697.

Wald, A. (1994). Modeling thermal infrared (2 – 14 μm) reflectance spectral of frost and snow, *Journal of Geophysical Research*, 99:24,241-24250.

Wan, Z. & Dozier, J. (1996). A generalized split-window algorithm for retrieving land surface temperature from space, *IEEE Transactions on Geoscience and Remote Sensing,* 34(4):892-905.

Wan, Z., Zhang, Y., Zhang, Q. & Li, Z.-L. (2002). Validation of the land-surface temperature products retrieved from Terra Moderate Resolution Imaging Spectroradiometer data. *Remote Sensing of Environment,* 83:163-180.

Wan, Z. (2008). New refinements and validation of the MODIS land-surface temperature/emissivity products, *Remote Sensing of Environment*, 112:59-74.

Wang, X. & Key, J. (2003). Recent trends in Arctic surface, cloud, and radiation properties from space, *Science*, 299(5613), 1725-1728.

Wang, X. & Key, J. (2005a). Arctic surface, cloud, and radiation properties based on the AVHRR Polar Pathfinder dataset. Part I: Spatial and temporal characteristics, *Journal of Climate*, 18(14):2558-2574.

Wang, X. & Key, J. (2005b). Arctic surface, cloud, and radiation properties based on the AVHRR Polar Pathfinder data set. Part II: Recent trends, *Journal of Climate*, 18(14), 2575-2593.

Yamaguchi, Y., Kahle, A.B., Tsu, H., Kawakami, T. & Pniel, M. (1998). Overview of advanced spaceborne thermal emission reflectance radiometer, *Geoscience and Remote Sensing*, 36:1062-1071.

Zwally, H. J. (& 15 others) (2002). ICESat's laser measurements of polar ice, atmosphere, ocean, and land, *Journal of Geodynamics,* 24:405-445.

TABLES

1. Spectral range and spatial resolution of TIR bands on MODIS, ASTER and ETM+ that are used to derive the LSTs discussed in this paper. Earth Science Data Type (ESDT) refers to the name of the MODIS and ASTER standard products.

2. Data corresponding with Figures 4, AWS and ASTER, MODIS and ETM+ LST comparison. There are 10 AWS-MODIS comparisons and 11 AWS-ETM+ comparisons; one ASTER and one ETM+ pixel each, are used for the one ASTER and ETM+ comparison. AWS acquisition times were interpolated to match MODIS acquisition times.

FIGURES

1. Greenland Climate Network (GC-Net) automatic weather station (AWS) location map of Greenland (from Steffen and Box, 2001).

2. Hourly air temperatures vs. surface temperatures in 2000 and 2001 for Summit Station, Greenland.

3a. Map view of two specific ICESat altimetry profiles across the Flade Isblink ice cap in northeastern Greenland. The approximate center coordinates of Flade Isblink ice cap are 81° 34' N, 15° 0' W. Elevations from ICESat Track 0045 were acquired on 02/25/04 and elevations from ICESat Track 0248 were acquired on 03/10/04 during Laser 2B operations period. The surface elevations derived from these ICESat tracks are shown in the above right graphs, and the black vertical bars show the approximate start and end of the ice surface. Plotted with the elevations are surface temperatures derived from the MOD11A1 product for 3 July 2001. The entire ice cap surface is close to the melting point, so the surface temperature does not vary with elevation.

3b. ASTER true color (left) and land surface temperature (LST) (right) images of North Ice Cap on 23 June 2004 are shown. ASTER and MODIS surface temperatures derived from along the transect shown on the ASTER LST image are plotted. The transect starts in the north and ends in the south. The approximate center coordinates of North Ice Cap are 76° 55' N, 68° 00' W.

4. Comparisons of satellite-derived and in-situ AWS LSTs. MODIS-derived and in-situ AWS LSTs are compared for 10 cases; ETM+ and AWS-derived LSTs are compared for 11 cases; and one case shows a comparison of ASTER and in-situ AWS LSTs. Four MODIS and four corresponding ETM+ scenes, and one ASTER scene were used to develop the graph.

5. Illustration of the comparison between MODIS-derived LST and AWS-derived air temperature in cases where the AWS air temperature should equal the LST. Excluded are cases when downward solar irradiance exceeded 240 W m^{-2} while wind speed was <4 m s^{-1}. Also excluded are cases when AWS air temperatures were above the melting point. The solid line is the 1:1 line. The dashed line is the best-fit line.

6. MODIS – ASTER comparison. Seven MODIS and seven corresponding ASTER scenes were used to develop the plot using three scenes from the Greenland Ice Sheet. 65 cases are plotted. The solid line is the 1:1 line. The dashed line is the best-fit line.

7a. MODIS and ETM+ comparison, where emissivity = 0.98 in the ETM+ LST calculation. The solid line is the 1:1 line. The dashed line is the best-fit line.

7b. MODIS and ETM+ comparison, where emissivity = 0.99 in the ETM+ LST calculation. The solid line is the 1:1 line. The dashed line is the best-fit line.

Table 1. Spectral range and spatial resolution of TIR bands on MODIS, ASTER and ETM+ that are used to derive the LSTs discussed in this paper. Earth Science Data Type (ESDT) refers to the name of the MODIS and ASTER standard products.

Instrument (ESDT)	**Band number and (spectral range) in μm**	**Pixel size**
MODIS (MOD11_L2)	31 (10.780 - 11.28) 32 (11.770 - 12.27)	1 X 1 km
ASTER (AST08)	10 (8.125 – 8.475) 11 (8.475 – 8.825) 12 (8.925 – 9.275) 13 (10.25 – 10.95) 14 (10.95 – 11.65)	90 X 90 m
ETM+	6 (10.31 – 12.36)	57 X 57 m

Table 2. Data corresponding with Figure 4 - AWS and ASTER, MODIS and ETM+ LST comparison. There are 10 AWS-MODIS comparisons and 11 AWS-ETM+ comparisons; only one ASTER and one ETM+ pixel each, are used for the ASTER and ETM+ comparison. AWS acquisition times were interpolated to match MODIS acquisition times.

Date	AWS Station	AWS LST (°C)	ETM+ LST (°C) Avg.	Std Dev of ETM+ Avg.	No. of Pixels Averaged	MOD11_L2 LST (°C)	Δ AWS – ETM+ Avg. LST (°C)	Δ AWS – MODIS LST (°C)	ETM+ Acquisition Time (UTC)	MODIS Acquisition Time (UTC)	Distance from Nadir (MODIS) (km)
7/7/2001	Crawford Pt 1	0.51	-0.55	0.46	1306	-0.17	1.06	0.68	14:50	15:25	79.05
8/1/2001	Crawford Pt 1	-4.52	-4.18	0.49	1258	-3.51	-0.34	-1.01	14:43	15:15	30.28
6/29/2000	DYE-2	-3.05	-6.34	0.46	1271	-2.91	3.29	-0.14	14:34	15:15	93.54
8/3/2001	DYE-2	-4.00	-2.11	0.42	1277	-1.71	-1.89	-2.29	14:31	15:05	100.51
6/8/2000	NASA-E	-10.78	-10.16	0.43	1251	-10.05	-0.62	-0.73	14:13	14:50	5.04
6/4/2001	NASA-SE	-15.00	-11.98	0.45	1219	-12.75	-3.02	-2.25	14:07	14:40	1.01
6/28/2000	NASA-U	-7.21	-5.92	0.43	1282	-5.79	-1.29	-1.42	15:28	16:05	54.72
7/2/2000	NGRIP	-7.43	-10.08	0.43	1257	-10.65	2.65	3.22	15:03	15:40	0.00
9/6/2001	Saddle	-14.42	-14.37	0.45	1290	-15.37	-0.05	0.95	14:19	14:50	64.58
8/4/2000	South Dome	-9.33	-6.39	0.49	1265	-7.15	-2.94	-2.18	14:10	14:50	21.15

Date	AWS Station	AWS LST (°C)	ETM+ LST (°C)		ASTER LST (°C)	Δ AWS – ETM+ LST (°C)	Δ AWS – ASTER LST (°C)	ETM+ Acquisition Time (UTC)	ASTER Acquisition Time (UTC)	
7/2/2001	Summit	-12.50	-10.08		-10.85	-2.42	-1.65	14:30	15:06	

Figure 1

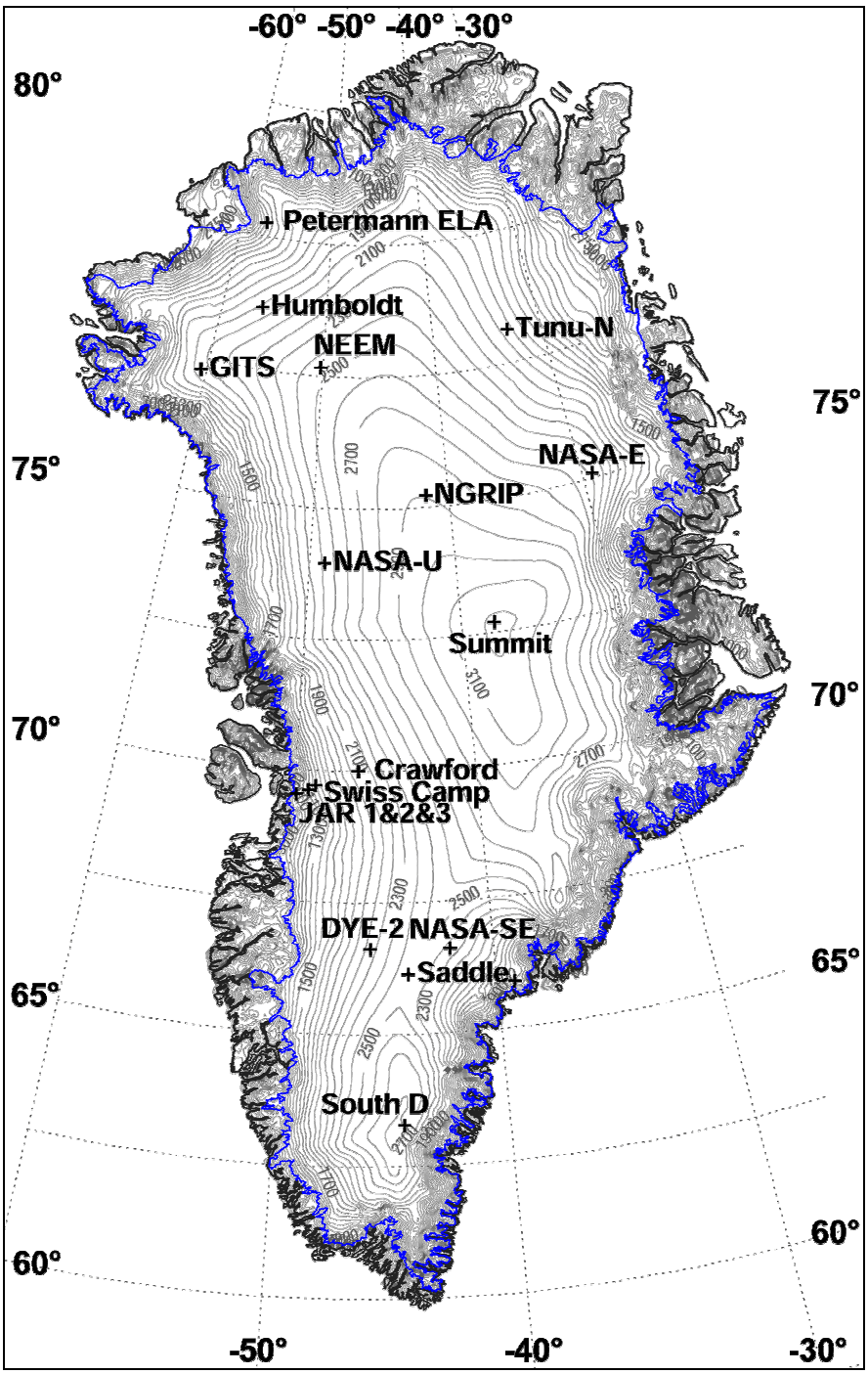
-60° -50° -40° -30°
80°
75°
70°
65°
60°
-50°
-40°
-30°
+ Petermann ELA
+Humboldt
NEEM
+GITS
+Tunu-N
NASA-E
+NGRIP
+NASA-U
Summit
+ Crawford
+ Swiss Camp
JAR 1&2&3
DYE-2
NASA-SE
+Saddle
South D

Figure 2

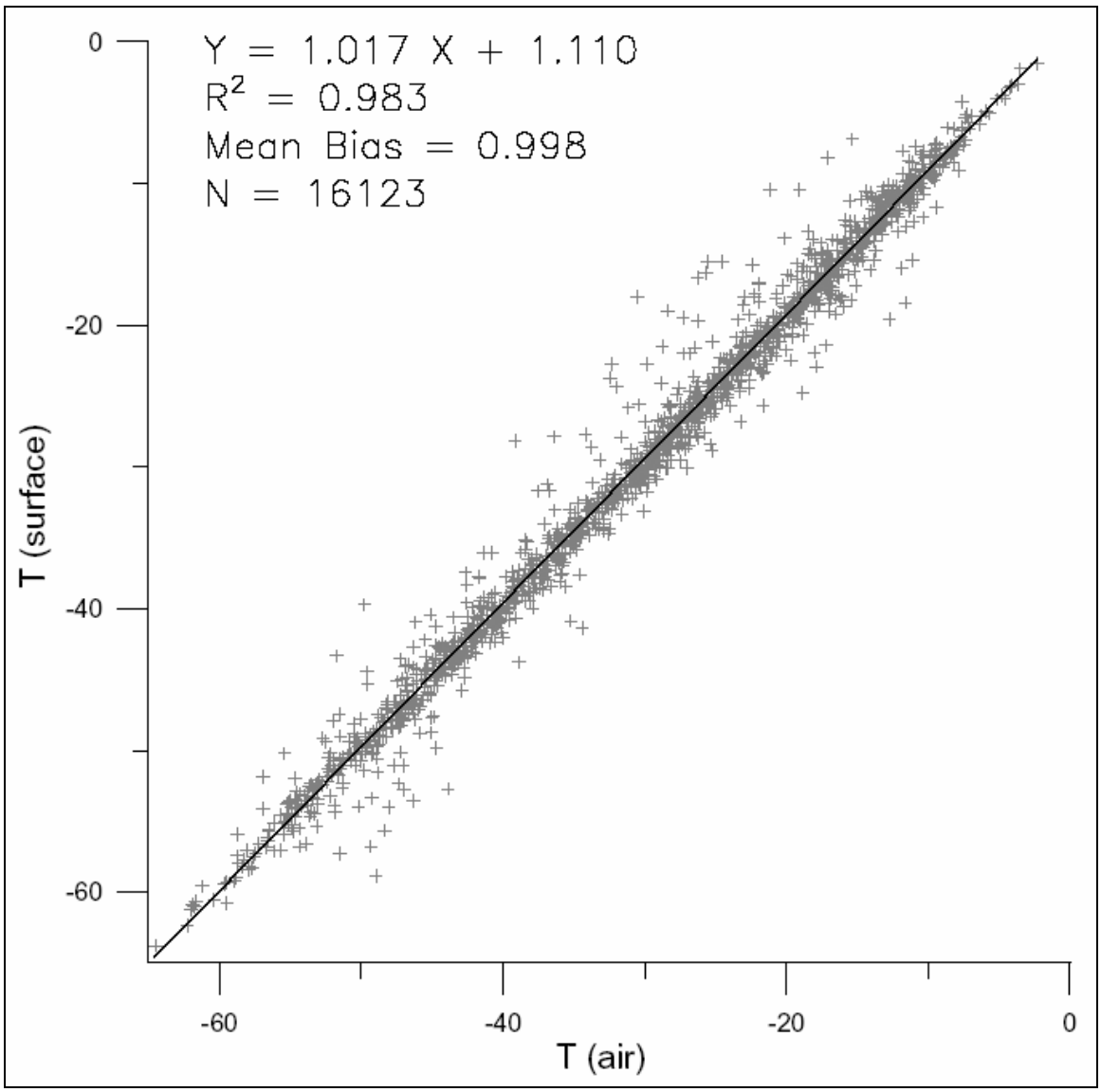
Y = 1.017 X + 1.110
R2 = 0.983
Mean Bias = 0.998
N = 16123
0
-20
-40
-60
T (surface)
-60
-40
-20
0
T (air)

Figure 3a

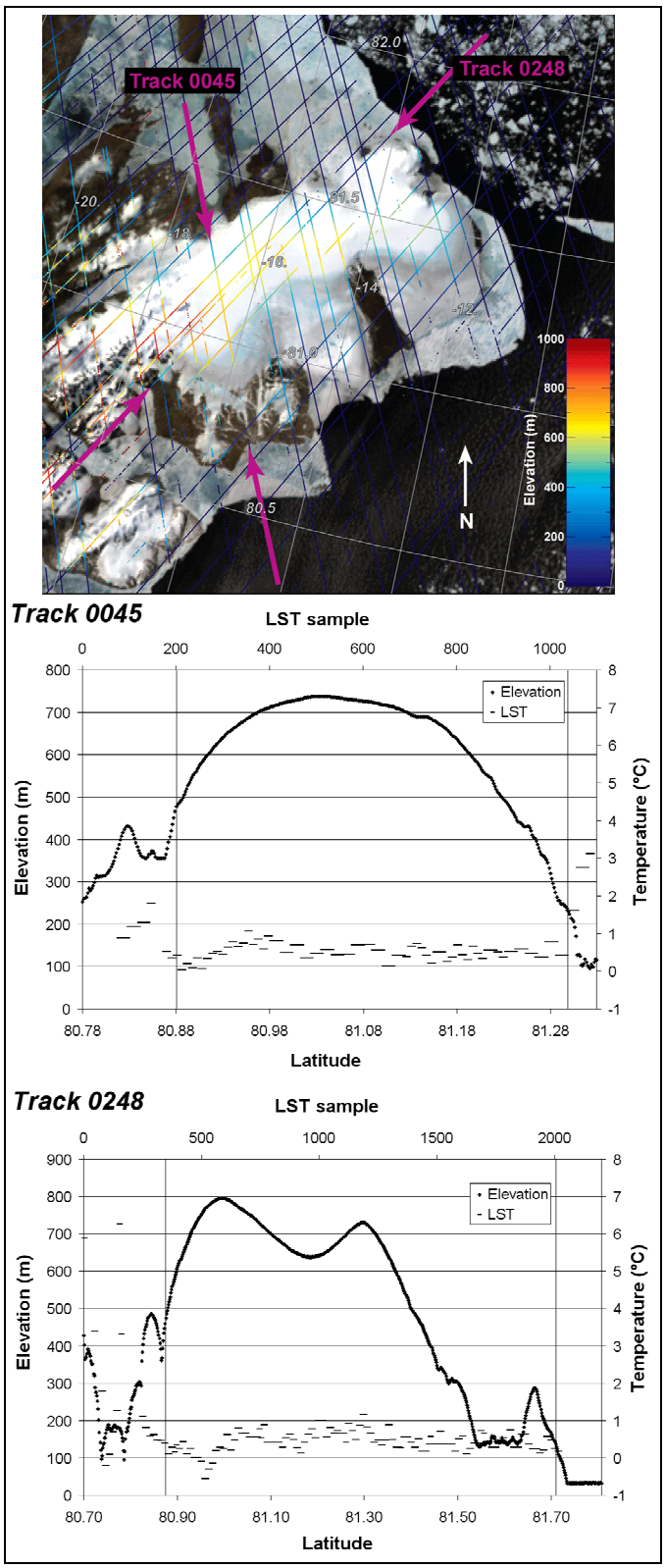
Track 0045
Track 0248
82.0
81.5
81.0
80.5
-20
-18
-16
-14
-12
N
Elevation (m)
1000
800
600
400
200
0
Track 0045
LST sample
Elevation
LST
Elevation (m)
Temperature (°C)
Latitude
0
200
400
600
800
1000
80.78
80.88
80.98
81.08
81.18
81.28
Track 0248
LST sample
Elevation
LST
Elevation (m)
Temperature (°C)
Latitude
0
500
1000
1500
2000
80.70
80.90
81.10
81.30
81.50
81.70

Figure 3b

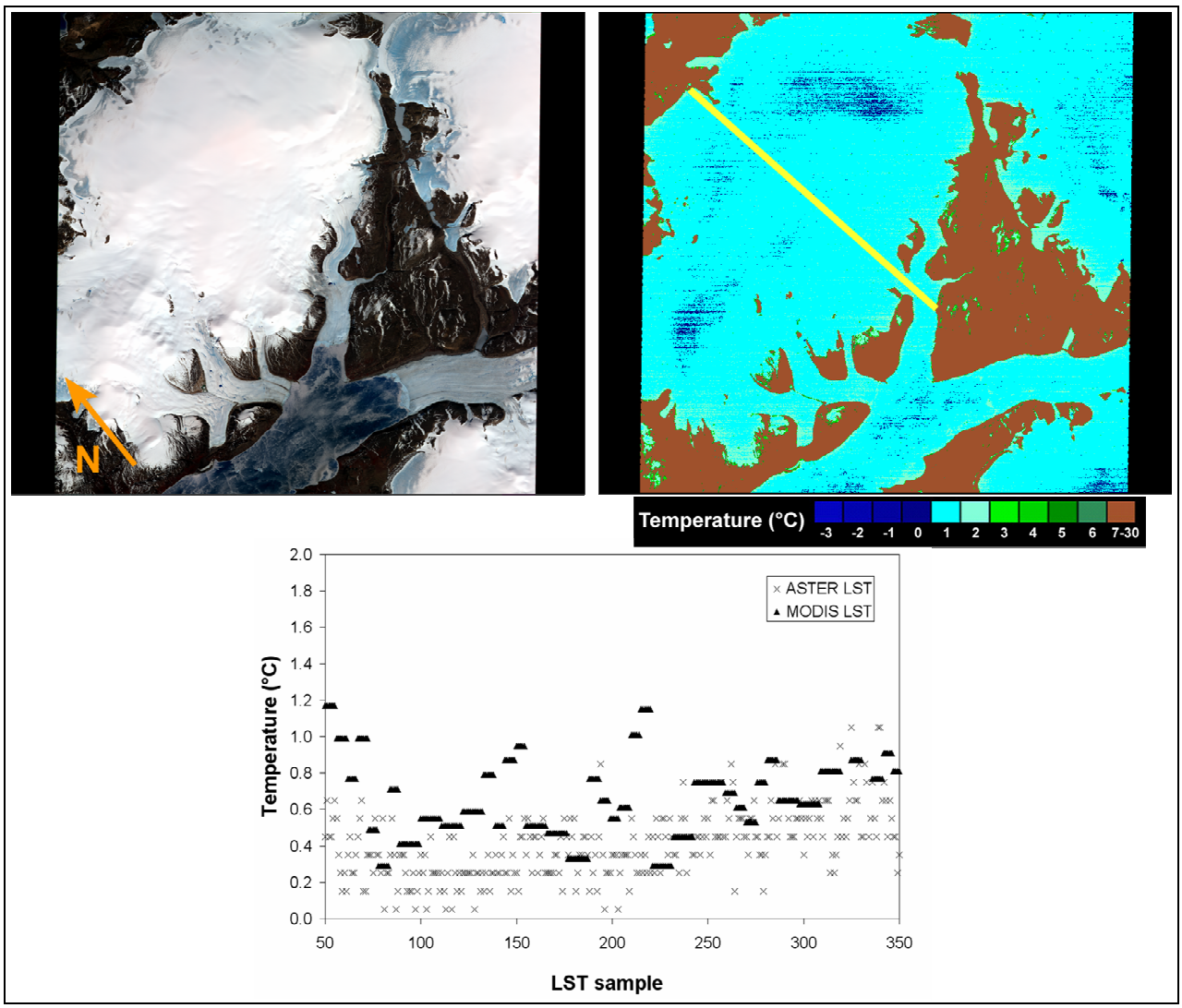
N
Temperature (°C)
-3 -2 -1 0 1 2 3 4 5 6 7-30
ASTER LST
MODIS LST
Temperature (°C)
LST sample
0.0 0.2 0.4 0.6 0.8 1.0 1.2 1.4 1.6 1.8 2.0
50 100 150 200 250 300 350

Figure 4

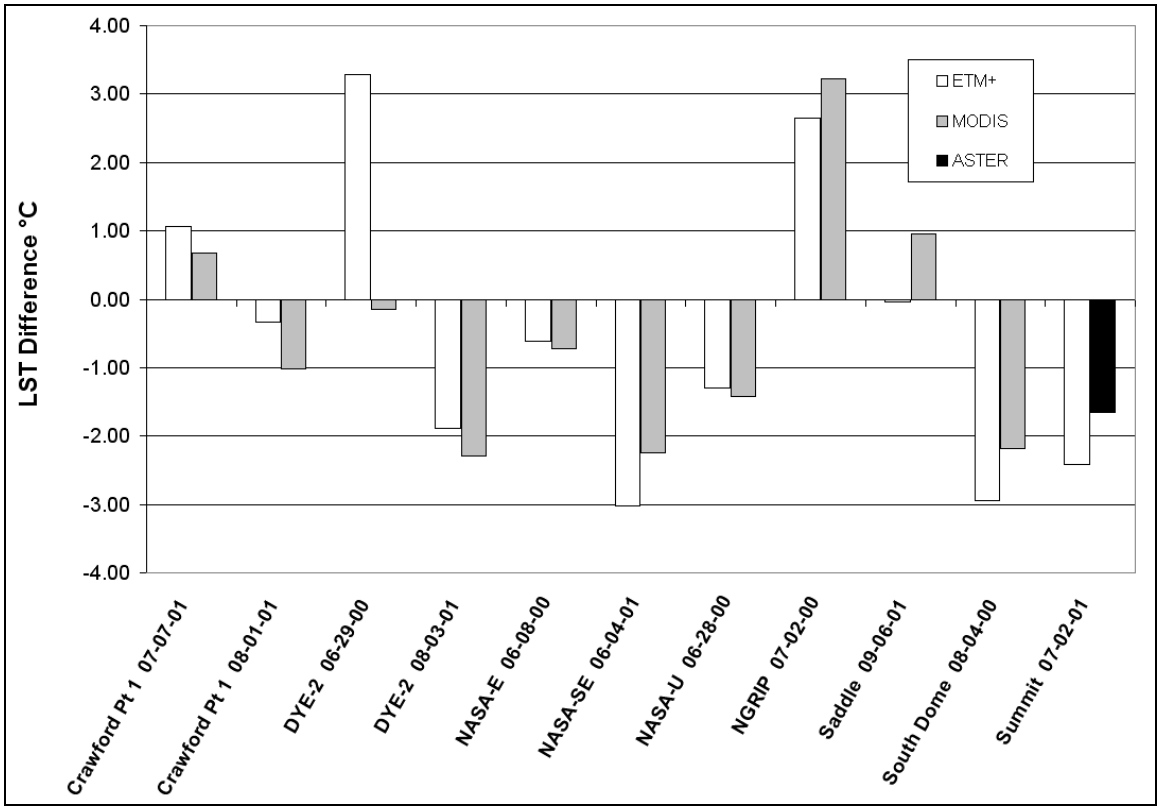
LST Difference °C
4.00
3.00
2.00
1.00
0.00
-1.00
-2.00
-3.00
-4.00
ETM+
MODIS
ASTER
Crawford Pt 1 07-07-01
Crawford Pt 1 08-01-01
DYE-2 06-29-00
DYE-2 08-03-01
NASA-E 06-08-00
NASA-SE 06-04-01
NASA-U 06-28-00
NGRIP 07-02-00
Saddle 09-06-01
South Dome 08-04-00
Summit 07-02-01

Figure 5

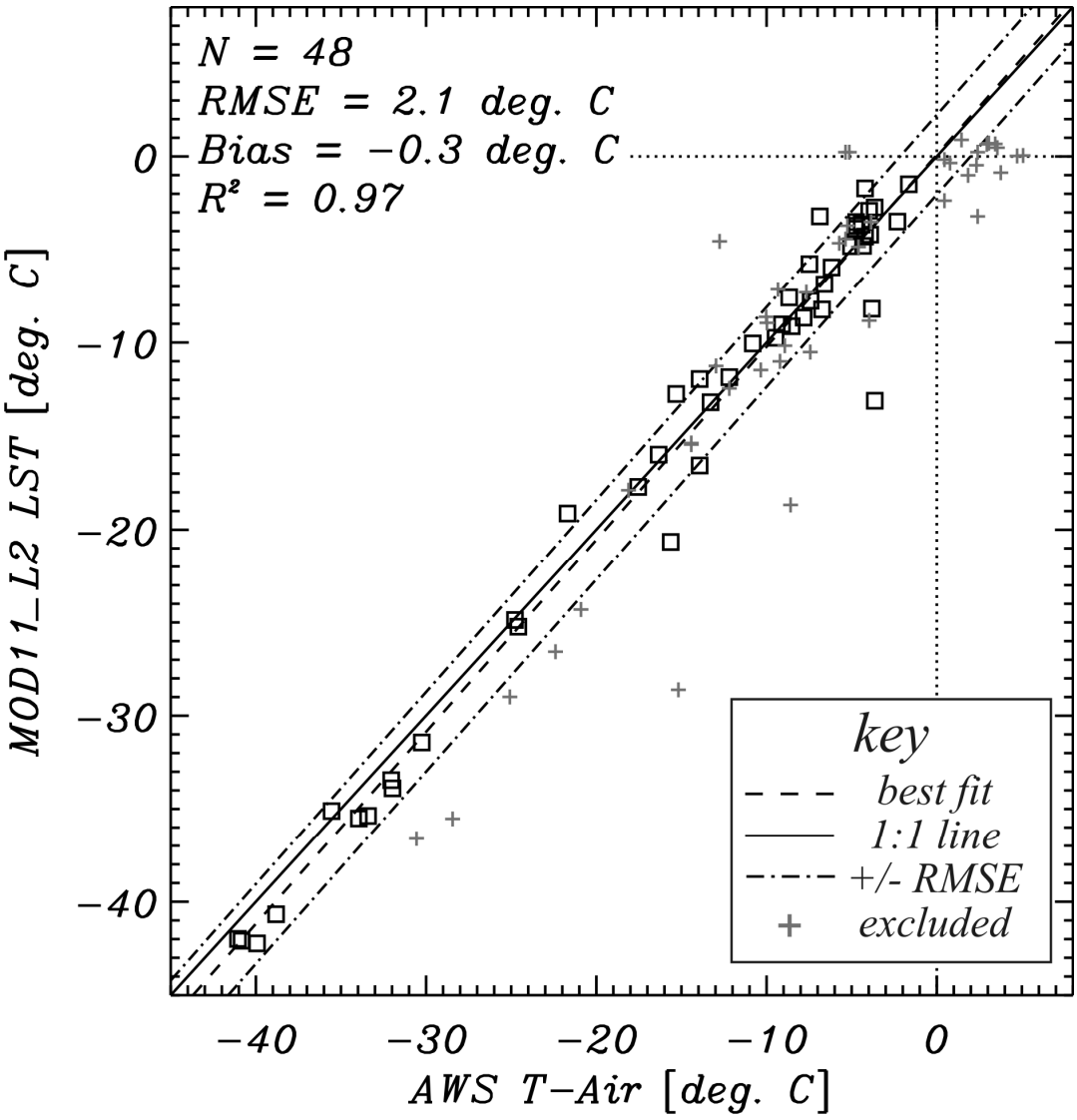
N = 48
RMSE = 2.1 deg. C
Bias = −0.3 deg. C
R² = 0.97
0
−10
−20
−30
−40
MOD11_L2 LST [deg. C]
−40
−30
−20
−10
0
AWS T−Air [deg. C]
key
best fit
1:1 line
+/- RMSE
excluded

Figure 6

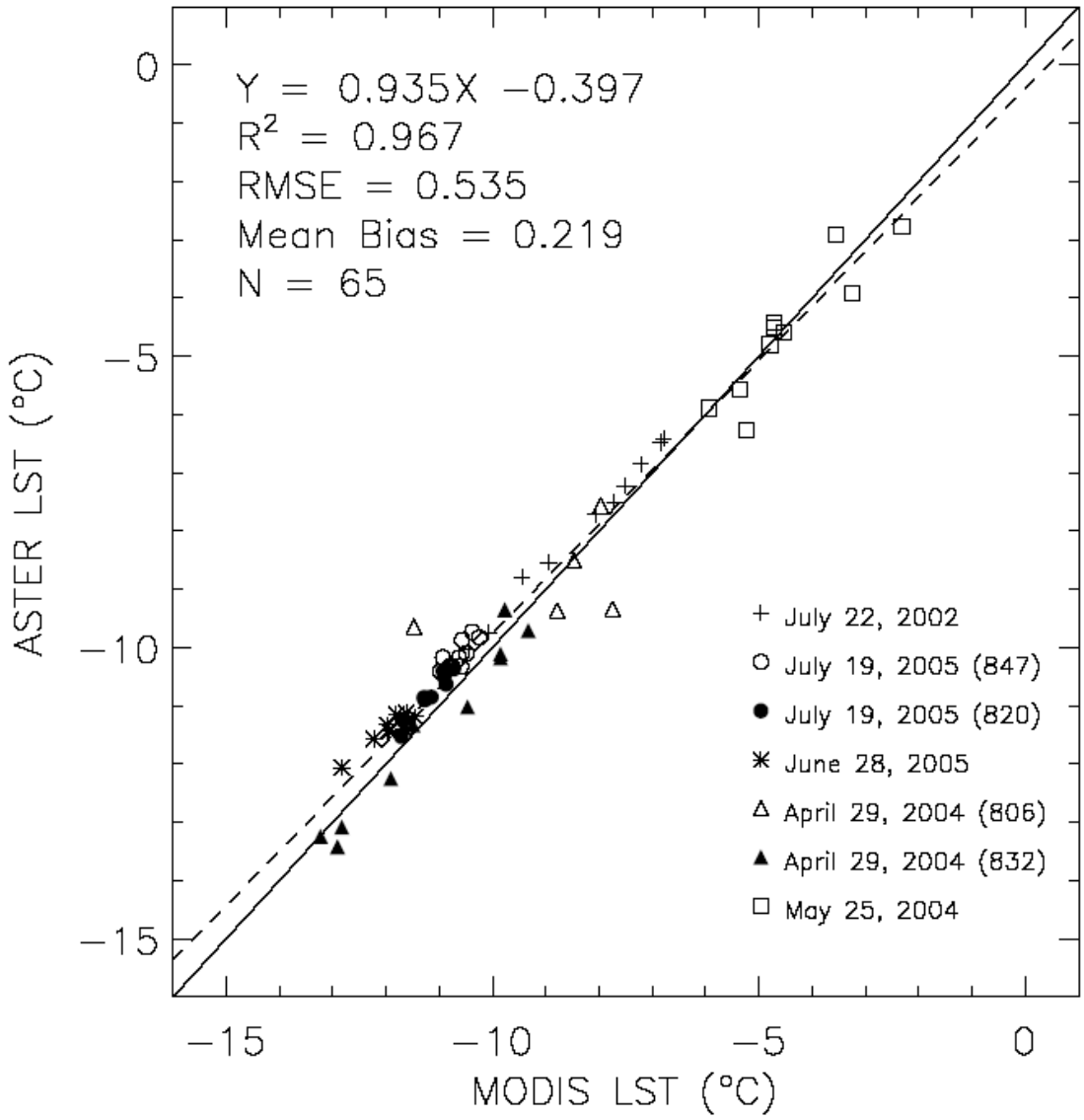
Y = 0.935X −0.397
R² = 0.967
RMSE = 0.535
Mean Bias = 0.219
N = 65
July 22, 2002
July 19, 2005 (847)
July 19, 2005 (820)
June 28, 2005
April 29, 2004 (806)
April 29, 2004 (832)
May 25, 2004
ASTER LST (°C)
MODIS LST (°C)
0
−5
−10
−15

Figure 7a

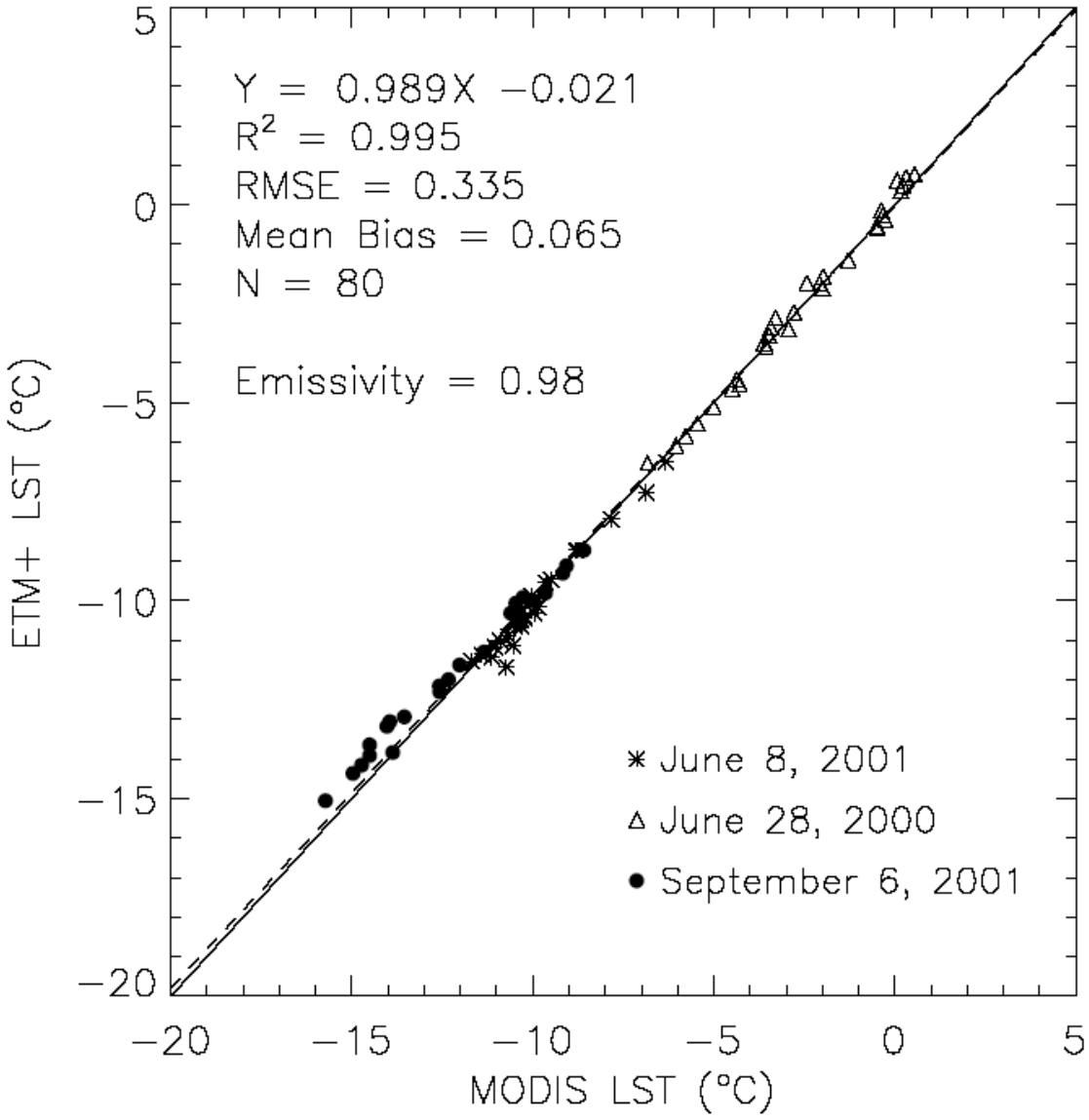
Y = 0.989X −0.021
R² = 0.995
RMSE = 0.335
Mean Bias = 0.065
N = 80
Emissivity = 0.98
June 8, 2001
June 28, 2000
September 6, 2001
ETM+ LST (°C)
MODIS LST (°C)
5
0
−5
−10
−15
−20
−20
−15
−10
−5
0
5

Figure 7b

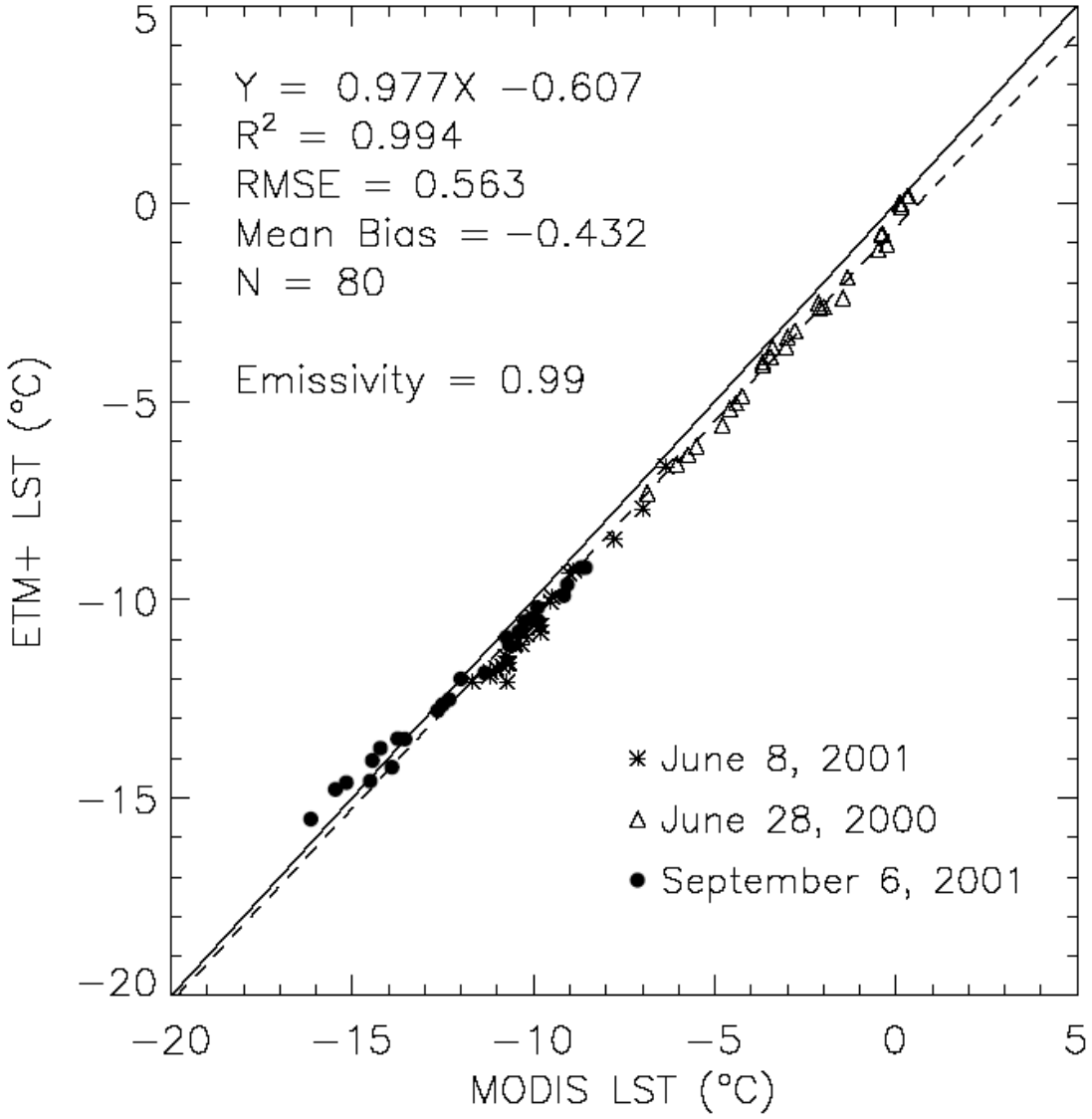
Y = 0.977X −0.607
R² = 0.994
RMSE = 0.563
Mean Bias = −0.432
N = 80
Emissivity = 0.99
June 8, 2001
June 28, 2000
September 6, 2001
ETM+ LST (°C)
MODIS LST (°C)
5
0
−5
−10
−15
−20